JOURNAL OF GUIDANCE, CONTROL, AND DYNAMICS
Vol. 33, No. 3, May–June 2010

Orbit Tuning of Planetary Orbiters for Accuracy Gain in Gravity-Field Mapping

Jaroslav Klokočník* and Aleš Bezděk†
Academy of Sciences of the Czech Republic, 251 65 Ondřejov, Czech Republic
Jan Kostelecký‡
Czech Technical University in Prague, 166 29 Prague 6, Czech Republic
and
Josef Sebera§
Academy of Sciences of the Czech Republic, 251 65 Ondřejov, Czech Republic

DOI: 10.2514/1.46223

When measurements from the Earth artificial satellites Gravity Recovery and Climate Experiment (devoted to the study of Earth's gravity field) were analyzed, it was discovered that there is a direct relationship between the density of satellite ground tracks D and the accuracy A of the gravity-field parameters derived from the satellite orbit(s) (in particular, of the monthly solutions for variable geopotential); the lower the D, the lower the A. This is due to passage of the satellite orbit through a low-order orbital resonance. A lesson learned from the Gravity Recovery and Climate Experiment was applied to the Gravity-Field and Steady-State Ocean Circulation Explorer; namely, the necessity of avoiding close proximity of its orbit (kept, in this case, at constant altitudes for the measurement phases with a gradiometer on board) to the 16:1 resonance. To avoid the decrease in A, we have to choose the orbit in such a way that order B of the lowest-order resonance, which will occur, will be higher than the highest degree $L_{\max}$ of spherical harmonic expansion of the potential already known for the particular body. For the Earth, $L_{\max}$ is now 150 [European improved gravity model of the Earth by new techniques (EIGEN-5S)] for satellite-only solutions and 2190 (Earth gravitational model 2008) for combination models. We extend these findings for a hypothetical future low-flying Mars orbiter; small changes in the semimajor axis can result in a dramatic improvement in accuracy of the derived gravity-field parameters, without any additional costs. The situation for Mars is similar to that of Earth. However, slowly rotating bodies like the moon, Mercury, or Venus do not yet suffer from similar problems because, for them, we obtain $L_{\max} < B$.

Nomenclature

A	=	design matrix of the linear model
a	=	mean semimajor axis of the satellite orbit, m
$\bar{C}_{lm}$, $\bar{S}_{lm}$	=	normalized Stokes parameters
D	=	density of the ground tracks at the equator, m
GM	=	planetocentric gravity constant, $\mathrm{km}^3\,\mathrm{s}^{-2}$
g	=	radial acceleration for a Mars orbiter, $\mathrm{m\,s}^{-2}$
I	=	mean orbit inclination, deg
J_2	=	zonal second-degree harmonic coefficient (Stokes parameter) related to the polar flattening of the planet in unnormalized form
$L_{\max}$	=	maximum degree of Stokes parameters or their time variations
M_0	=	mean anomaly (and its time derivative, the rate of M_0), deg
n	=	satellite's mean motion (revolutions per day)
n_{obs}	=	number of observations in the experiments with covariance matrices
n_{par}	=	number of solved-for parameters in the experiments with covariance matrices
o	=	circumference of the planet around the equator, m
$\bar{P}_{lm}(\cos\theta)$	=	normalized associated Legendre functions of the first kind
R	=	radius or best fitting (rotational) ellipsoid (expressing the shape of the planet), m
r	=	radius vector of the satellite, m
$\dot{S}$	=	rotational speed of the planet (revolutions per days on the planet)
SP	=	normalized Stokes parameters, $\bar{C}_{lm}$ and $\bar{S}_{lm}$
T_{zz}	=	the second radial derivative of the geopotential, m**E**
α	=	nodal days (number of revolutions of the planet with respect to the orbital plane)
β	=	nodal revolutions (number of satellite revolutions around the planet with respect to the ascending node)
θ	=	colatitude of the satellite, deg
λ	=	longitude of the satellite, deg
ψ_{lmpq}	=	phase in Lagrange planetary equations (degree l, order m, other indices p and q), deg
Ω	=	ascending node (and its time derivative, the rate of Ω), deg
ω	=	distance of periapsis from the ascending node (and its time derivative, the rate of ω), deg, deg/day

Received 2 July 2009; revision received 29 January 2010; accepted for publication 31 January 2010.

*Senior Scientist, Astronomical Institute, Galaxies and Planetary Systems, Fričova 298; jklokocn@asu.cas.cz.

†Postdoctoral Fellow, Astronomical Institute, Galaxies and Planetary Systems, Fričova 298; bezdek@asu.cas.cz.

‡Professor and Faculty of Civil Engineering, Department of Advanced Geodesy, Thákurova 7; kost@fsv.cvut.cz.

§Graduate Student, Astronomical Institute, Galaxies and Planetary Systems, Fričova 298; josef.sebera@fsv.cvut.cz.

I. Introduction

EARTH artificial satellites are a very useful tool to study the gravitational field of the Earth due to their worldwide and continuous observations by various methods. Their orbit determination and consequent computation of the harmonic geopotential coefficients (Stokes parameters) defining the Earth's gravitational field enable the creation of so-called Earth gravitational (or geopotential) models (EGMs) [1,2].

Recently, combined EGMs based on satellite data from the Challenging Minisatellite Payload (CHAMP) for geophysical research and application (GFZ/DLR) and the Gravity Recovery and Climate Experiment (GRACE) (NASA/DLR), along with a detailed, nearly global network of terrestrial gravity anomalies, provide a very precise and detailed description of the gravitational field. These EGMs have precision on the order of decimeters in geoid undulations, few milliGals in gravity anomalies, and several milliEötvös in the second derivatives of the geopotential (components of the Marussi tensor) on the majority of places on the globe [2]. Such results have many applications in astrodynamics, geodesy, geodynamics, geophysics, and other disciplines. Further progress in the EGMs is expected with the forthcoming data from the recently launched Gravity-Field and Steady-State Ocean Circulation Explorer (GOCE) mission (ESA), which is, for the first time, equipped with a space gradiometer (a set of microaccelerometers) enabling in situ measurements of the second derivatives of the gravitational potential [3].

For these missions, the orbit choice and design are crucial. Gravitational field missions are preferably put on low and nearly circular orbits to ensure high and constant sensitivity to the gravitational signal. Also very important is the choice of inclination of the orbital plane with respect to the plane of the Earth's equator, often selected as nearly polar, retrograde, and sun synchronous.

The mission orbit designers considered various aspects of orbit selection according to diverse applications of the satellites. Sometimes, requirements posed by the scientific community were in conflict. As an example, for altimetry missions, geodesists preferred freely decaying orbits, whereas oceanographers wanted orbits with a select stable height of flight (exact repeat orbits at resonances) with necessary active orbit keeping. This controversy has been solved in an optimum way for all users of the altimetry data, but not all details of orbit choices and their impact on scientific data of various kinds are well known and tested. For GRACE, it happened that the accuracy of gravitational-field variations (namely, of the monthly solutions since the mission's launch in 2002) suddenly decreased in the fall of 2004; although the method, data accuracy, and processing remained unchanged (Fig. 1[¶]). After the fall of 2004, the accuracy increased again to the original level. This phenomenon has been studied and explained in [4]; it is a result of an encounter of GRACE with the 61:4 orbit resonance (61 nodal revolutions of the satellite during four nodal days, a condition for exact repeat orbit), which led to a significant temporary decrease of the satellite ground-track density. As GRACE continues to fall in the atmosphere, a similar situation will repeat in the future [5].

From GRACE, we learned how to choose the appropriate orbit for GOCE (i.e., by making small changes to the semimajor axis) that would avoid any similar decrease in accuracy in the gravity products generated from the gradiometer measurements. GOCE was launched in a nearly circular and nearly sun-synchronous orbit at the initial height of 285 km. During its first free-decay phase in orbit, the satellite is supposed to pass through the 16:1 resonance (at 268.4 km). The effect of this resonance, together with the uncertainty in the solar activity prediction, has a distinct impact on the evolution of the orbital elements. Then, the so-called measurement operational phases (two planned phases, three optional) with the gradiometer will follow. To maintain a near-constant and extremely low altitude for these phases, the satellite will use an ion thruster to compensate for the atmospheric drag. To obtain a ground-track grid dense enough for a proper sampling of the gravitational field, ESA set the constraint for a minimum ground-track repeat period to two months. We studied suitable repeat cycles (resonant orbits) in the vicinity of the 16:1 resonance. We found that they differ greatly in stability toward small perturbations of the satellite's mean altitude and in the temporal evolution of the ground-track coverage. So, not only the orbit choice to avoid the 16:1 resonance but also the proper orbit tuning in its vicinity (about a kilometer above or below the 16:1 resonance) can significantly affect the quality of the output from the gradiometer [6].

[¶]Private communications with S. Bettadpur, 2004 and 2006.

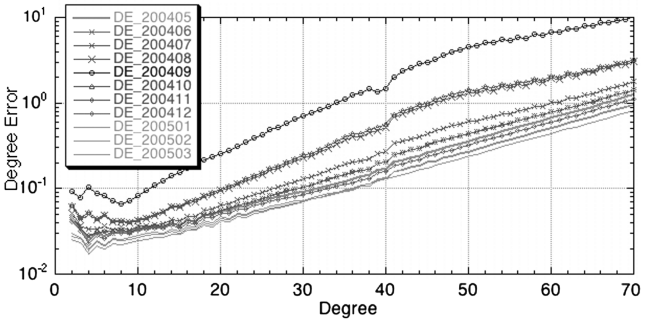

Fig. 1 Accuracy of the monthly solutions for the geopotential variations from May 2004 to March 2005. Note the remarkable accuracy decrease between August and October 2004. On the *x* axis, there is a degree of harmonic expansion of the gravity-field variations. Note the logarithmic scale on the *y* axis with the error of geoid height in millimeters (see footnote [¶]).

The same method can be extended, with some caution, to the lunar and planetary orbiters intended to study the gravitational fields of the moon and the planets. But, we have to distinguish between celestial bodies with slow rotation rates (e.g., the moon, Mercury, and Venus) and fast rotation rates (e.g., Earth and Mars), because the resonant phenomena for the slowly rotating bodies and their close orbiters are different from what we are accustomed to around the Earth. We offer a short outline of the cases of the GRACE and GOCE missions (see Sec. II.A) [4–6]. After a generalization (Sec. II.B), we present numerical results for a possible future low orbiter around Mars (Sec. II.C). With small changes in the height of a Mars orbiter, one can easily achieve much better gravity-field description in terms of precision and resolution. A discussion of Venus, Mercury, and the moon will enlighten the situation for these bodies (in Sec. II.D).

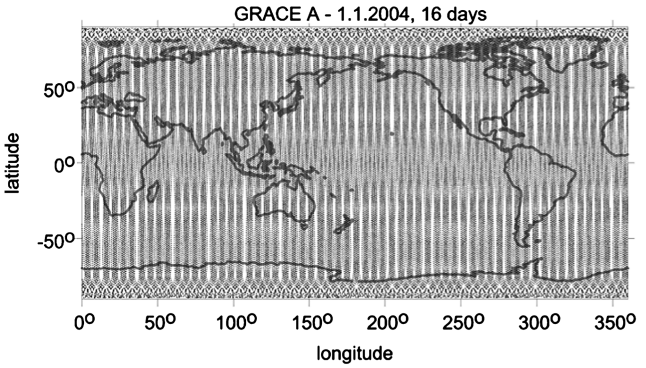

a)

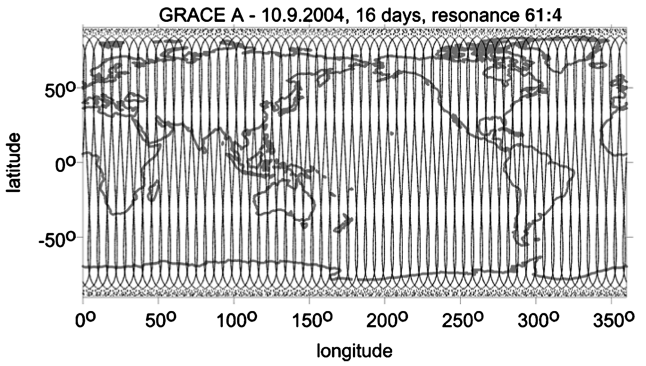

b)

Fig. 2 Ground tracks of GRACE A a) well before (January 2004) and b) at the exact 61:4 orbit resonance (September 2004). At the 61:4 resonance, the density *D* is a) about 100 km and b) 660 km . These density differences perfectly correlate with the accuracy changes of the monthly solutions shown in Fig. 1.

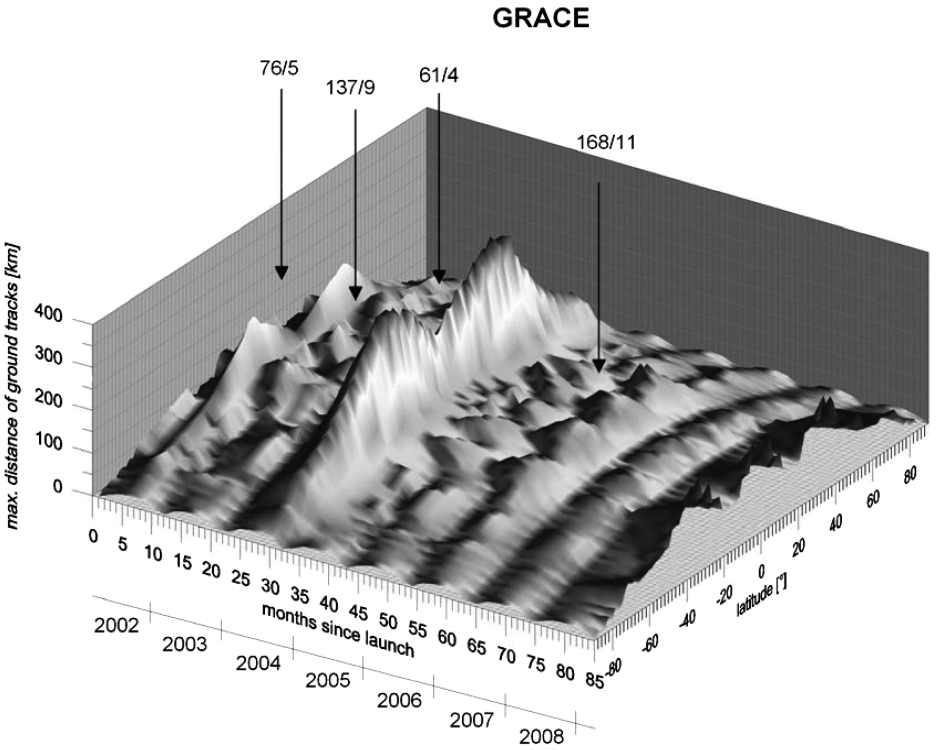

Fig. 3 Evolution of the ground-track density for GRACE since its launch in 2002 until spring 2009, shown here in the form of maximum distance of ground tracks in kilometers.

II. Density of Ground Tracks Versus Accuracy of Gravity Results

A. Gravity Recovery and Climate Experiment to Gravity-Field and Steady-State Ocean Circulation Explorer

In a short outline, we first present the observed fact (Fig. 1) that the evolution of the accuracy of the monthly solutions for the geopotential variations derived from the GRACE data. The accuracy decreased from 200405 (May 2004) to 200409 (September 2004) by about one order of magnitude, whereas the quality of the data and methodology was the same; then, the accuracy increased back to the previous level (March 2005, curve 200503 in Fig. 1).

The explanation of why this happened came from a study of the resonant phenomena of artificial Earth satellites [7–9] and was presented in [4,5]. When the satellite performs $\boldsymbol{\beta}$ nodal revolutions around the planet during $\boldsymbol{\alpha}$ nodal days (i.e., synodic with respect to the orbital plane), we speak about $\boldsymbol{\beta}$:$\boldsymbol{\alpha}$ resonance. The numbers $\boldsymbol{\alpha}$ and $\boldsymbol{\beta}$ are mutually prime integers [7] (i.e., the ratio $\boldsymbol{\beta}$:$\boldsymbol{\alpha}$ must be irreducible). The physical meaning of the orbit resonance is that the satellite returns after $\boldsymbol{\beta}$ revolutions exactly above the same place of the planet (i.e., the satellite ground track starts to repeat). These resonant phenomena were used to determine some characteristics of the gravity field of the Earth (e.g., [8,9]) and the orbit choice of oceanographic exact repeat missions (ERMs), or geodetic missions in the case of altimetry satellites [10]. For the gravity-field studies of the Earth (determination of the lumped geopotential coefficients), such low-order resonances as the 15:1, 29:2, 31:2, or 61:4 were used in the past (e.g., [11]); to define ERMs for satellite altimetry, such orbits as 43:3 or 127:10, and 244:17 or 501:35 were selected (see [12] and references in that book).

The density of ground tracks at the equator is $\boldsymbol{D} = \boldsymbol{o}/\boldsymbol{\beta}$, where the circumference $\boldsymbol{o} = 40,075$ km (for the Earth). The quantity $\boldsymbol{D}$ can also be described as the longitudinal spacing of adjacent tracks at the equator [10,12]. It should be distinguished from the longitudinal spacing between the sequential orbit traces at the equator, sometimes called the fundamental interval, $\boldsymbol{F} = \boldsymbol{o\alpha}/\boldsymbol{\beta}$ (not used in this paper).

The core of the problem can be described as follows. At a low-order resonance (i.e., when $\boldsymbol{\beta}$ is small, say 15, 31, or 47), the density of the ground tracks $\boldsymbol{D}$ is much lower (order-of-magnitude differences) than in the general case (at a high-order resonance, say 200). Then, we can have the same quality and amount of satellite observations for the gravity-field determination, but their spatial distribution (in latitude and longitude) is much poorer (Figs. 2a and 2b). This is the reason for a lower accuracy of gravity-field products. The phenomenon of the accuracy decrease is temporary; due to the atmospheric drag (caused by very low but not negligible density of the upper atmosphere), the semimajor axis (height of flight) of the satellite is steadily decreasing; thus, the density of the ground tracks is changing with time.

The problem with a drop of the accuracy of the monthly solutions, based on the GRACE data, has been solved and may now look trivial, but it was not so trivial a few years ago, as Fig. 1 and works [4,5,13] confirm.

The evolution of the ground-track density for GRACE is visible in Fig. 3, in which we show its dependence on time (month by month) together with the dependence on latitude (compare to Fig. 10a in [5]). This figure is based on the actual orbital elements of GRACE (A). After one low-order resonance, another low-order resonance may occur. There are remarkable differences in the density (not percents, but multiples) during that time interval, with a minima of density at the resonances. The lower the order of resonance, the lower the density of the ground tracks (which means higher values on the *y* axis on this graph). Also, the dependence on latitude is enormous. Note that the minimum density is not at the equator (it is not a general rule; it depends on orbit inclination). Sources for the mean orbital elements are the GFZ/DGFI two-line elements on ftp.gfz-potsdam.de and ftp://ftp.dgfi.badwmuenchen.de/pub/laser/predictions/GRACE_PRED/, since the launch until May 2009. It is also obvious from the graphs (resonant diagrams) in Figs. 6, 7, and 15 in [5] for GRACE, CHAMP, and GOCE, and in more detail in [6] for GOCE (we will not repeat these graphs for the Earth satellites in this paper; here, we will focus on resonant diagrams for selected planetary orbiters).

B. Generalization

An experience with GRACE will now get more theoretical background. Then, this will be applied generally to the planetary orbiters (Secs. II.C and II.E).

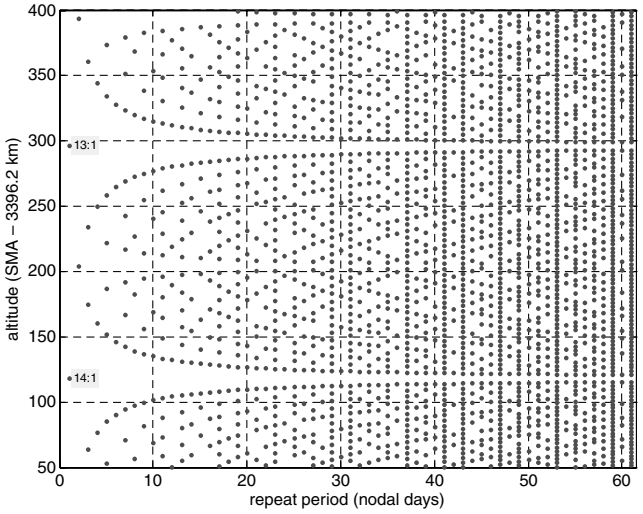

a)

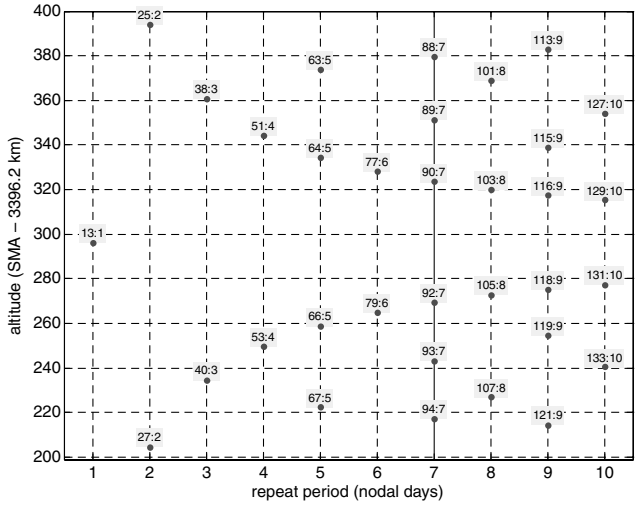

b)

Fig. 4 Resonance diagrams for Mars orbiter with nominal inclination of 92.7 deg and orbit heights between a) 50 and 400 km and b) 200 and 400 km (a zoom for the lowest repeat periods up to $\alpha = 10$). (SMA denotes semimajor axis.)

Recalling the exact resonance $\boldsymbol{\beta}$:$\boldsymbol{\alpha}$, the phase ψ_{lmpq} in the Lagrange planetary equations (LPEs) (e.g., [7]) at the exact resonance becomes $\dot{\psi} = 0$. The relevant satellite mean motion $\boldsymbol{n}$ can then be derived as

$$n = \frac{\beta}{\alpha}(|\dot{S}| - \dot{\Omega}) - \dot{\omega} - \dot{M}_0 \tag{1}$$

Now, we have to put the LPEs for the orbital elements $\boldsymbol{\Omega}$, $\boldsymbol{\omega}$, and $\boldsymbol{M_0}$ into Eq. (1); we get [5,6]

$$n = \frac{\beta}{\alpha}|\dot{S}|\left\{1 + zJ_2\left(6\cos^2 I - \frac{3}{2} \pm \frac{3}{2}\frac{\beta}{\alpha}\cos I\right)\right\}; \qquad z = \left(\frac{R}{a}\right)^2$$

where the minus sign is valid for the normal rotation of the planet, and the plus sign is valid for the retrograde rotation of the planet. Finally, we arrive at

$$n = \frac{\beta}{\alpha}|\dot{S}|\left\{1 - \frac{3}{2}J_2\left(\frac{R}{a}\right)^2\left(4\cos^2 I - \tau\frac{\beta}{\alpha}\cos I - 1\right)\right\} \tag{2}$$

where $\dot{S} > 0$ for $\tau = 1$, and $\dot{S} < 0$ for $\tau = -1$: the former case for the normal rotation and the latter case for the retrograde rotation. Note that $J_2 = -\sqrt{5}\bar{C}_{20}$.

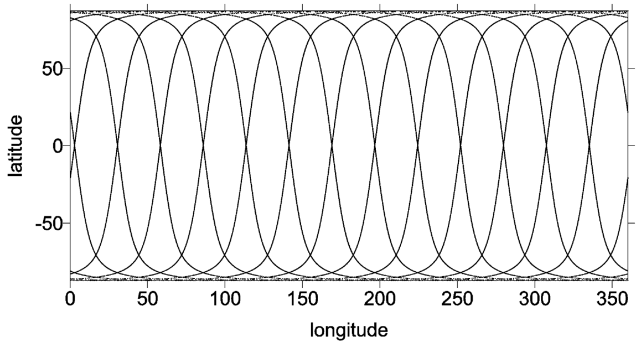

a)

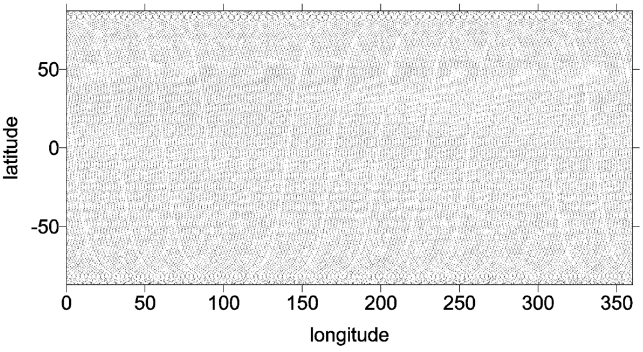

b)

Fig. 5 Ground tracks for a Mars orbiter at the 13:1 and 188:15 resonances to compare D and to estimate a possible loss of accuracy due to a hypothetically bad choice of orbit (too close to the 13:1 or similar low-order resonance). The density D at 13:1 is 1640 km, D at 188:15 is approximately 110 km.

The first case, with $\tau = 1$, is the traditional condition known since Allan [7] or Gooding [8], when the so-called lumped geopotential coefficients from the resonances of the Earth's artificial satellites were determined. The second case, $\tau = -1$, is valid for the retrograde rotation of a planet (Venus, in this study), so that Eq. (1) is a generalized equation for the resonant mean motion (or relevant mean semimajor axis) as a function of $\boldsymbol{I}$ and $\boldsymbol{\beta}$:$\boldsymbol{\alpha}$. We will not deal with the details of how to compute $\boldsymbol{a}$ from $\boldsymbol{n}$ and which type of $\boldsymbol{a}$ it should be (e.g., Kozai's, Brouwer's, t averaged, or other; for a detailed explanation, see [14]).

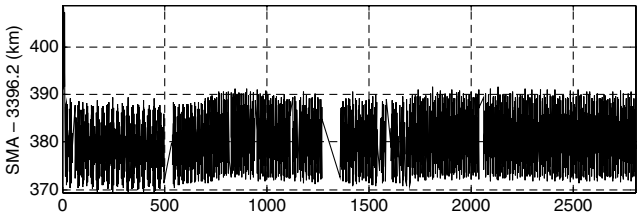

a)

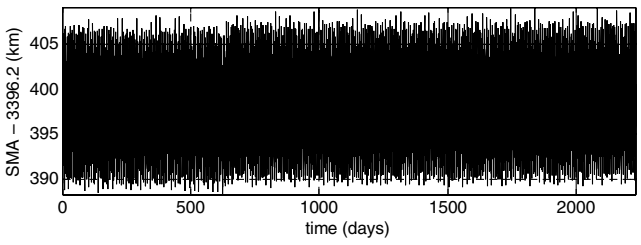

b)

Fig. 6 Time evolution of osculating semimajor axis of a) MGS and b) ODY orbiters of Mars (data with courtesy of G. Balmino, Centre National d'Etudes Spatiales).

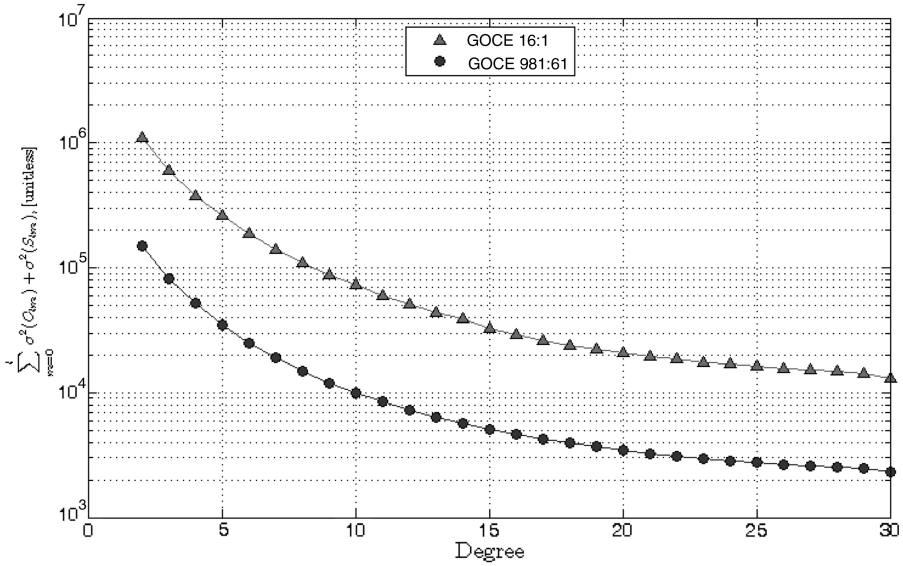

Fig. 7 Degree error variances for two simulated orbit scenarios for GOCE.

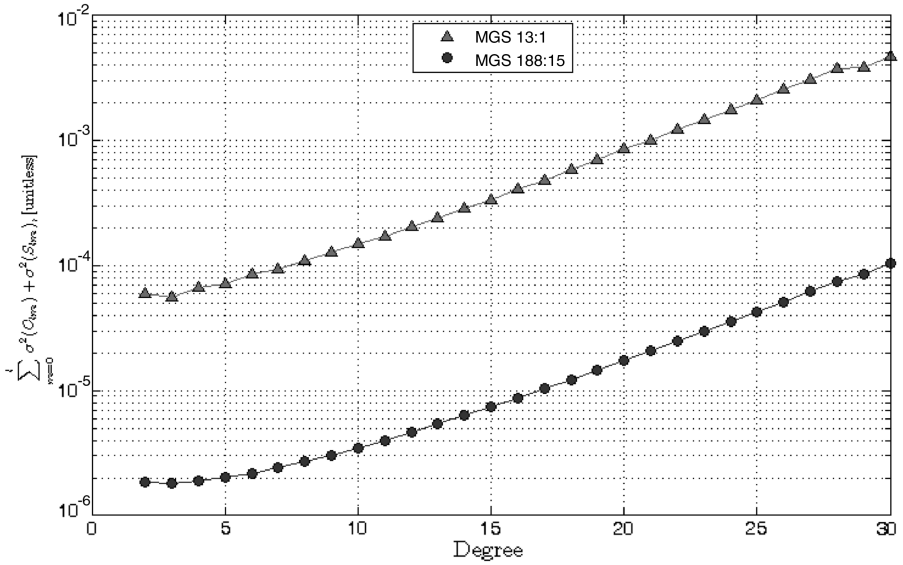

Fig. 8 Degree error variances for two simulated orbit scenarios for Mars orbiter.

Now, we can better understand the resonance evolution diagrams on Fig. 4. On the x axis, we have the repeat period of $\boldsymbol{\alpha}$ nodal days and on the y axis there is the mean semimajor axis; each graph point corresponds to a resonance and is labeled with the number $\boldsymbol{\beta}$ of the satellite nodal revolutions. These graphs are valid only for the particular inclination. However, the results are, not too sensitive for orbit inclination (the graphs would shift only a little in the y axis for a few degrees of change in the inclination). They are valid for effectively circular orbits (too-eccentric orbits are not optimum for gravity-field studies).

As time passes, the semimajor axis of the Earth's satellite contracts due to the atmospheric drag, and the satellite orbit undergoes the resonances in the graph from top to bottom. Obviously, at each instant, we can find a high-order resonance (large $\boldsymbol{\beta}$ and relevant $\boldsymbol{\beta}$:$\boldsymbol{\alpha}$), which has no practical sense from the view of the study of the gravity field, nor from the viewpoint of oceanographic applications.

For the first time, we suggested this type of graph in Deutsches Geodätisches Forschungsinstitut (DGFI), Munich, cooperating on the orbit choice (called, at that time, the orbit dossier) of the ESA altimetry mission Earth resources satellite (ERS)-1 [15]. Before, another graphical representation of resonance evolution was used [16]. Recently, our types of graphs have appeared in [17]. The resonant graphs not only show which resonances will be encountered during the free fall, or which ERM should be selected for oceanography, but they can also suggest which orbits should be avoided (see the case of GOCE in [6]).

These graphs cannot quantitatively display the previously mentioned relationship of the density of ground tracks versus the accuracy of gravity products. This was solved experimentally and with a covariance projection in the case of satellite-to-satellite tracking between GRACE A/B [5]. We deal with this topic in Sec. II.D.

The question is how the resonant diagrams will look like for various planetary orbiters. We assume low and circular orbits and orbiters intended to (also or solely) study the gravity field. First of all, we have to replace the values of $\boldsymbol{GM}$, $\boldsymbol{J_2}$, $\boldsymbol{R}$, and $\dot{S}$ (see Table 1). The values conform to the international standards defined in Seidelmann et al. [18]; they differ slightly from the older values in [17].

We also have to generalize the computation of the semimajor axis for $\boldsymbol{\beta}$:$\boldsymbol{\alpha}$ resonance to cover the case when the rotation of the planet is in the retrograde sense (Venus). This is done by Eq. (2). In the next section, we present the examples for Mars, and in Sec. II.E we present the results for the moon, Mercury, and Venus.

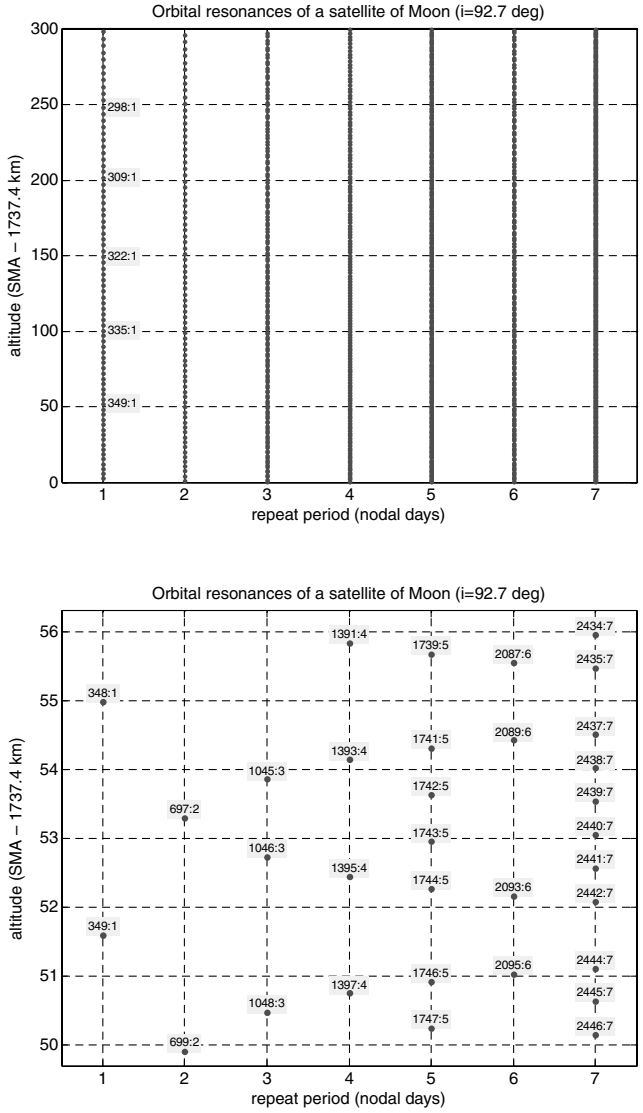

Fig. 9 Resonant diagram (top) and its zoom (bottom) for low and nearly polar orbits of the moon orbiter.

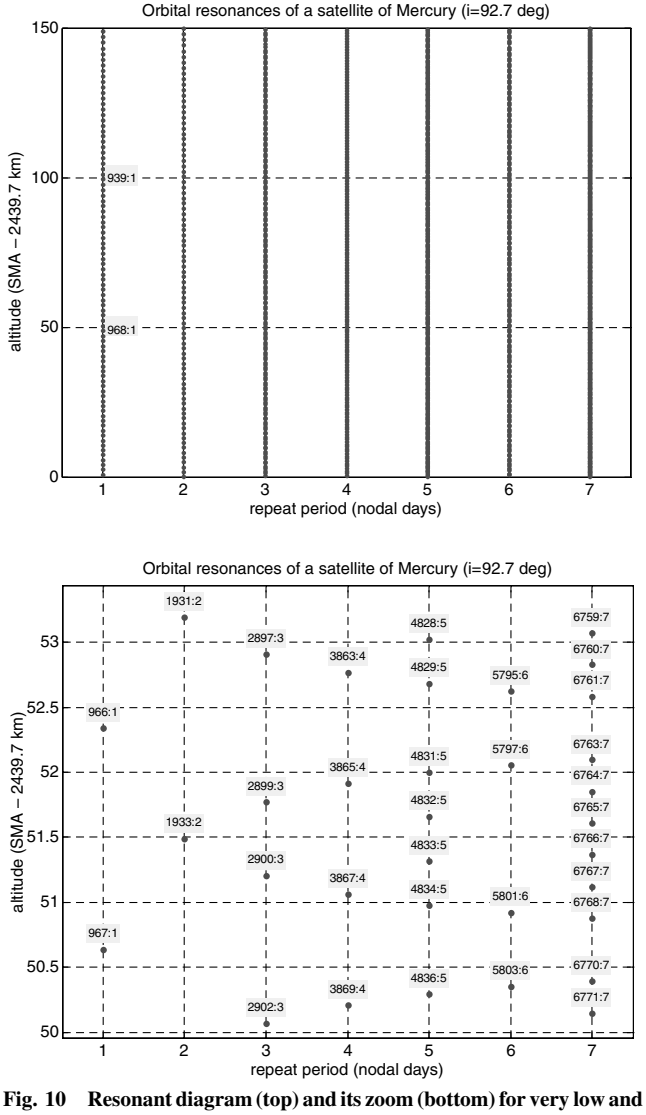

Fig. 10 Resonant diagram (top) and its zoom (bottom) for very low and nearly polar orbits of a Mercury orbiter.

It should be noted that we focus only on the resonance phenomenon and its relationship to the quality of the gravity-field products and not on the actual orbit determination, which (for these bodies) may be complicated by significant $\boldsymbol{m}$-daily perturbations and third-body effects.

For the planetary and lunar orbiters, we have Table 2 as a partial guide of satellite missions that have already been completed or are prepared; it gives us an idea about the orbit choice of these missions and projects.

C. Mars Orbiter

The Mars gravity-field model from the Mars Global Surveyor (MGS) data Goddard Mars Model (GMM)-2B extends to $\boldsymbol{L}_{\max} = 60$ in degree and order [19]. With MGS and Mars Odyssey (ODY) data together, the newest gravity-field model MGGM08A goes to the degree and order of 90 [20].

The theory and generally valid information are given in the previous sections. The examples follow. The resonant diagram for close Mars orbiters shows a situation similar to that around the Earth; we can put a satellite into an orbit in the vicinity of a low-order orbit resonance, like 13:1, 14:1, or 25:2, and consequently lose a certain degree of accuracy in the gravity-field products (Fig. 4). It may well happen, like for the Earth satellites, that $\boldsymbol{L}_{\max} > \boldsymbol{B}$ (here, the lowest possible orders $\boldsymbol{B}$ are about 12–14). The ground tracks for the 13:1 resonance are shown in Fig. 5a. The actual missions of MGS and ODY (see Table 2) had orbits with height variations (due to the orbit maneuvers, etc.) passing throughout various higher-order resonances (for example, 188:15) (Fig. 5b), so they were optimal (but not ideal) for the gravity-field determination. However, the permanent vicinity to the 25:2 resonance would be negative. The actual variations of osculating semimajor axes of MGS and ODY are shown in Figs. 6a and 6b. They demonstrate evolution of the actual orbits; in contrast to this, our examples (Figs. 4a and 4b) show possible choices for future hypothetical (low and nearly circular) orbits; some of them can be close to the orbits of MGS and ODY, but a much higher variety of orbit choices from the viewpoint of the gravity-field study are possible.

For future Mars orbiters (on nearly circular orbits), it is recommended to avoid low-order resonances, according to Figs. 4a and 4b (modified for the particular case according to the actual orbit inclination). Small changes in the semimajor axis (which may be already selected by the mission orbit designers to fulfill goals of the mission other than gravity-field determination) by a few kilometers, up or down, will lead to a substantial improvement in the accuracy of these parameters, almost without any additional cost.

D. Density Versus Accuracy: Simple Numerical Test Using Covariance Matrix

The connection between the accuracy degradation in the gravity-field modeling and the density of ground tracks may be shown by

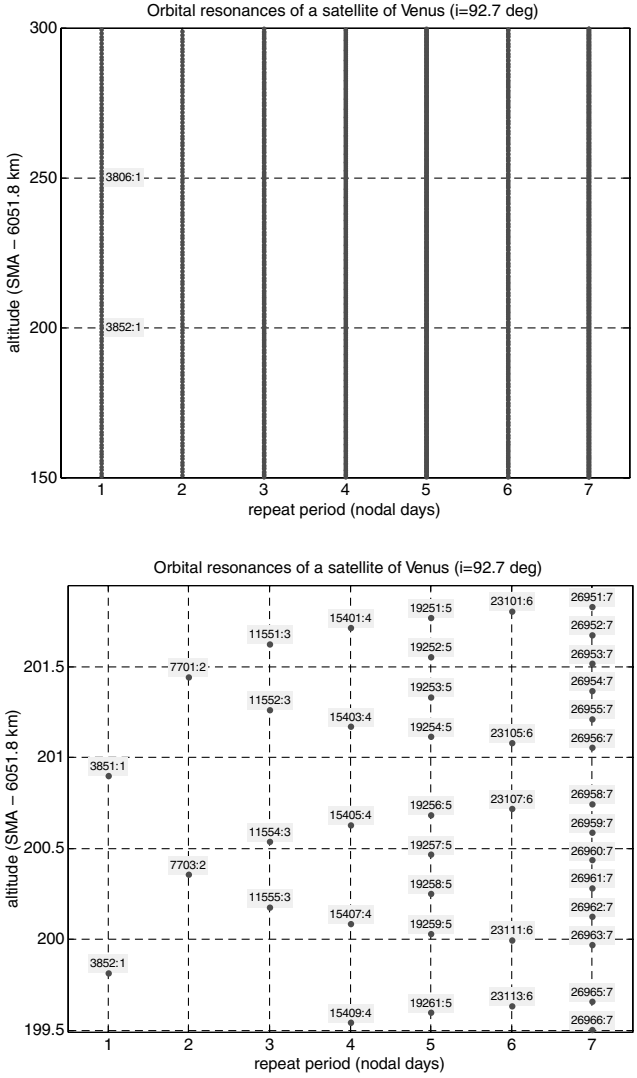

Fig. 11 Resonant diagram (top) and its zoom (bottom) for very low and nearly polar orbits of a Venus orbiter.

means of the covariance matrix of the simplified linear observation model. We present examples for missions around the Earth and Mars. In the first case, two hypothetical orbit settings for GOCE are considered: one at the exact low-order resonance of 16:1 and the other at a high-order resonance of 981:61. For simplicity, we assume that the GOCE data used as observables will only be the second radial derivative T_{zz} of the geopotential. In case of a hypothetical Mars orbiter, we used the gravity radial acceleration g as the presumed observable.

1. Case of Gravity-Field and Steady-State Ocean Circulation Explorer (Earth Satellite)

Let us consider T_{zz} in the spherical approximation as the measured quantity [21]:

Table 1 Basic dynamic parameters of the Earth and other bodies of the solar system

Body	GM, km^3 s^{-2}	J_2, 10^{-6}	R, m	$\dot{S}$, rev/day
Earth	398,600.44	1082.627	6,378,137	1.00274
Moon	4902.80	203.428	1,738,140	0.03660
Mercury	22,032.24	60	2,439,700	0.01705
Venus	324,858.36	5.97	6,051,800	−0.00411
Mars	42,828.37	1959.2	3,396,190	0.97470

$$T_{zz} = \frac{GM}{R^3}\sum_{l=2}^{L\max}\sum_{m=0}^{l}(l+2)(l+1)\left(\frac{R}{r}\right)^{l+3}(\bar{C}_{lm}\cos m\lambda + \bar{S}_{lm}\sin m\lambda)P_{lm}(\cos\theta) \tag{3}$$

For the corresponding design matrix $\boldsymbol{A}$ of the linear model, it holds that

$$A_{Tzz} = \begin{bmatrix} \frac{\partial T_{zz}(r_1,\theta_1,\lambda_1)}{\partial \mathrm{SP}_{2,0}} & \cdots & \frac{\partial T_{zz}(r_1,\theta_1,\lambda_1)}{\partial \mathrm{SP}_{L\max,L\max}} \\ \vdots & \ddots & \vdots \\ \frac{\partial T_{zz}(r_{n\mathrm{obs}},\theta_{n\mathrm{obs}},\lambda_{n\mathrm{obs}})}{\partial \mathrm{SP}_{2,0}} & \cdots & \frac{\partial T_{zz}(r_{n\mathrm{obs}},\theta_{n\mathrm{obs}},\lambda_{n\mathrm{obs}})}{\partial \mathrm{SP}_{L\max,L\max}} \end{bmatrix} \tag{4}$$

where the number of observations n_{obs} equals the number of points in the satellite ground tracks. Using the design matrix $\boldsymbol{A}$, we can simply simulate the influence of the ground-track density (representing the observation geometry) upon the accuracy of the SP via the covariance matrix,

$$\mathrm{cov}\,(\mathrm{SP}) = (A^T A)^{-1} \tag{5}$$

where the dimension of the covariance matrix equals $n_{\mathrm{par}} = (L_{\max})^2 + 2L_{\max} - 3$ (taking the minimum degree two). We suppose that the covariance matrix is diagonal with a unit-error variance for all the observations and, in this way, we will discuss only the relative precision of the results obtained from different orbital configurations.

Figure 7 shows the error degree variances [i.e., a sum of the diagonal elements of the covariance matrix in Eq. (5) with respect to degree l] of both hypothetical orbit scenarios for the GOCE mission (16:1 and 981:61). We want to show a significant difference in the accuracy for the different ground-track densities (Figs. 5a and 5b), although it is evident that the case with denser ground tracks (981:61) has lower standard deviations than the low-order resonance of 16:1 by almost one order of magnitude. More examples display the same effect: a higher spherical resolution leads to an even more significant difference in the accuracy.

2. Case of Mars Orbiter

Two types of orbits were tested for a low-flying Mars orbiter; namely, the repeat configurations 13:1 and 188:15, with the radial accelerations as the presumed observables. We applied the simple linear model [22],

$$g = -\frac{GM}{R^2}\sum_{l=2}^{L\max}\sum_{m=0}^{l}(l+1)\left(\frac{R}{r}\right)^{l+2}(C_{lm}\cos m\lambda + S_{lm}\sin m\lambda)P_{lm}(\cos\theta) \tag{6}$$

for which the corresponding design matrix $\boldsymbol{A}$ is now

$$A_a = \begin{bmatrix} \frac{\partial g(r_1,\theta_1,\lambda_1)}{\partial \mathrm{SP}_{2,0}} & \cdots & \frac{\partial g(r_1,\theta_1,\lambda_1)}{\partial \mathrm{SP}_{L\max,L\max}} \\ \vdots & \ddots & \vdots \\ \frac{\partial g(r_n,\theta_n,\lambda_n)}{\partial \mathrm{SP}_{2,0}} & \cdots & \frac{\partial g(r_n,\theta_n,\lambda_n)}{\partial \mathrm{SP}_{L\max,L\max}} \end{bmatrix} \tag{7}$$

Figure 8 displays our results for two orbit scenarios around Mars. Again, the observations with the lower ground-track density (resonance 13:1, Fig. 5a) give higher standard deviations than in the case with the higher ground-track density (resonance 188:15, Fig. 5b).

Using the relevant functionals for either the GOCE (T_{zz}) or the Mars orbiter (g), one can easily demonstrate an effect of the ground-track geometry (overall coverage by ground tracks) on the quality of the solution of potential coefficients, even if the low maximum resolution is used (here, $l_{\max} = 30$). Because the potential coefficients need to be estimated from the global coverage by measured data, it roughly holds: the denser the grid, the better the precision.

Table 2 List of the main moons and planetary orbiters (excluding the Earth) also used for gravity-field studies, including projects (status summer 2009)

Body	Name of mission	Date	Orbit height, km (periapsis × apoapsis)	Orbit inclination, deg
Moon	Clementine	>1994	2200 × 4600	90
Moon	Lunar Prospector	>1998	100	90.5
Moon	Selenological and Engineering Explorer	>2007	100	90
Moon	Lunar Reconnaissance Orbiter	>2008	30 × 70	90
Moon	Chang'e 1	2007–2009	200	64
Moon	Chandrayaan	>2008	From 500 to crash	90
Moon	Gravity Recovery and Interior Laboratory tandem, NASA	2011	50	90
Mercury	Messenger	>2008	Flybys	——
Mercury	BepiColombo, ESA	2013	400 × 1500	——
Venus	Pioneer Venus Orbiter	1980–1982	200 × 67,000 to burn up in atmosphere	150
Venus	Magellan	1990–1994	250	85.5
Venus	Venus Express	>2005	400 × 66,000	90
Mars	Mariner 9	>1971	——	——
Mars	Viking 1 and 2	>1978	——	——
Mars	MGS	>1997	400	92.7
Mars	ODY	>2002	400	93.1
Mars	Mars Express Orbiter	>2003	180	52
Mars	Mars Reconnaissance Orbiter	>2006	250 × 316	93

E. Slowly Rotating Bodies: the Moon, Mercury, and Venus

The resonant phenomena for the slowly rotating bodies and their orbiters in nearly circular orbits are different from what we are accustomed to around the Earth or Mars. We show examples computed with Eq. (2) for the moon, Mercury, and Venus.

To avoid a decrease in the accuracy of the gravity-field parameters, we have to choose the orbit in such a way that the order $\boldsymbol{B}$ of the lowest-order resonance will be higher than the highest degree $\boldsymbol{L}_{\max}$ of the spherical harmonic expansion of the potential already known for the particular body, $\boldsymbol{L}_{\max} < \boldsymbol{B}$. For the Earth, $\boldsymbol{L}_{\max} = 2190$ (gravity-field model EGM2008 [2]), for Mars, $\boldsymbol{L}_{\max} = 95$ [20], for Venus, $\boldsymbol{L}_{\max} = 180$ [22], for the moon, $\boldsymbol{L}_{\max} = 70$ [23], and for Mercury, $\boldsymbol{L}_{\max}$ is very low (derived from the flybys only). For GRACE, GOCE, and other Earth satellites, as well as for the Mars orbiters, we can imagine a situation when $\boldsymbol{L}_{\max} > \boldsymbol{B}$. For example, this corresponds to 61:4, or 31:2 for GRACE and 16:1 for GOCE. Note that there is a problem of resolvability from the resonance (repeat cycle) orbits that leads to a stronger condition (namely, $\boldsymbol{L}_{\max} < \boldsymbol{B}/\boldsymbol{2}$), but this is discussed elsewhere [4].

Now, we extend the analysis of resonant phenomena for slowly rotating bodies, like the moon, Mercury, or Venus. The resonance diagrams for them degenerate due to a slow rotation to stripes; a few of those are shown in Figs. 9a, 10a, and 11a. When we use a big zoom (with a short interval of semimajor axes on the y axis), then we can see graphs similar to those known for the Earth or Mars; examples are in Figs. 9b, 10b, and 11b. The lowest resonant orders for very low orbits are about 350, 970, and 3850 for the moon, Mercury, and Venus, respectively. Thus, we show that these bodies do not suffer from similar problems as the Earth or Mars, because they have $\boldsymbol{L}_{\max} < \boldsymbol{B}$.

III. Conclusions

A relationship between the ground-track density (which is dictated by the proximity to orbit resonances) and the accuracy of the gravity-field products has been discovered when studying the orbit behavior of GRACE. The lower the density, the lower the accuracy. The experience has been extended to GOCE. The extension to other celestial bodies of the solar system, provided in this paper, is then a logical step of analyses. For Mars, we find a situation similar to that for the Earth, and we suggest fine orbit tuning (which means small changes in semimajor axis) for a future close Mars orbiter mission to achieve maximum gain in the accuracy of the gravity-field parameters (and, namely, their time variations derived from the respective orbits). For the Earth and Mars, it is well possible that the lowest resonance orders B will be smaller than the maximum degree $L_{\max}$ of the gravity-field expansion to spherical harmonics already achieved for the Earth (∼150, 2190 for satellite-only gravitational field models and for models combined from satellite and terrestrial data, respectively) or Mars (∼100), so $L_{\max} > B$. We have to avoid orbits too close to the exact low order resonances. For slowly orbiting bodies like the moon, Mercury or Venus, the situation is different; they do not suffer from leakage of accuracy because here $L_{\max} < B$.

Acknowledgments

This work has been supported by grant ESA Plan for European Cooperating States C 98056. We thank Jan Vondrák (Astronomical Institute of the Academy of Sciences of the Czech Republic, Prague) for his consultations and data, Rune Floberghagen (ESA/European Space Research Institute, Frascati), and Frank G. Lemoine (NASA Goddard Space Flight Center, Greenbelt) for inspiring discussions. We also acknowledge one of the reviewers for the constructive comments leading to an improvement of the paper.

References

[1] Förste, C., Flechtner, F., Schmidt, R., Stubenvoll, R., Rothacher, M., Kusche, J., Neumayer, H., Biancale, R., Lemoine, J. M., Barthelmes, F., Bruinsma, S., Koenig, R., and Meyer, U., "EIGEN-GL05C: A New Global Combined High-Resolution GRACE-Based Gravity Field Model of the GFZ-GRGS Cooperation," *Geophysical Research Abstracts*, Vol. 10, Abstract EGU2008-A-03426, Copernicus Publ., Göttingen, Germany, 2008.

[2] Pavlis, N. K., Holmes, S. A., Kenyon, S. C., and Factor, J. K., "An Earth Gravitational Model to Degree 2160: EGM2008," *Geophysical Research Abstracts*, Vol. 10, Abstract EGU2008-A-01891, Copernicus Publ., Göttingen, Germany, 2008.

[3] ESA GOCE, http://www.esa.int/goce [retrieved 30 June 2009].

[4] Wagner, C. A., McAdoo, D., Klokočník, J., and Kostelecký, J., "Degradation of Geopotential Recovery from Short Repeat-Cycle Orbits: Application to GRACE Monthly Fields," *Journal of Geodesy*, Vol. 80, No. 2, 2006, pp. 94–103. doi:10.1007/s00190-006-0036-x

[5] Klokočník, J., Wagner, C. A., Kostelecký, J., Bezděk, A., Novák, P., and McAdoo, D., "Variations in the Accuracy of Gravity Recovery due to Ground Track Variability: GRACE, CHAMP, and GOCE," *Journal of Geodesy*, Vol. 82, No. 12, 2008, pp. 917–927. doi:10.1007/s00190-008-0222-0

[6] Bezděk, A., Klokočník, J., Kostelecký, J., Floberghagen, R., and Gruber, C., "Simulation of Free Fall and Resonances in the GOCE Mission," *Journal of Geodynamics*, Vol. 48, No. 1, 2009, pp. 47–53. doi:10.1016/j.jog.2009.01.007

[7] Allan, R. R., "Satellite Resonance with Longitude-Dependent Gravity, 3: Inclination Changes for Close Satellites," *Planetary and Space*

Science, Vol. 21, No. 2, 1973, pp. 205–225.
doi:10.1016/0032-0633(73)90007-X

[8] Gooding, R. H., "Lumped Fifteenth Order Harmonics in the Geopotential," *Nature Physical Science*, Vol. 231, No. 5299, May 1971, pp. 168–169.

[9] Kostelecký, J., and Klokočník, J., "Collocations and the Thirtieth Order Resonant Harmonics," *Planetary and Space Science*, Vol. 31, No. 8, Aug. 1983, pp. 829–841.
doi:10.1016/0032-0633(83)90136-8

[10] Parke, M. E., Steward, R. H., and Farless, D. L., "On the Choice of Orbits for an Altimeter Satellite to Study Ocean Circulation and Tides," *Journal of Geophysical Research*, Vol. 92, No. C11, 1987, pp. 11693–11708.
doi:10.1029/JC092iC11p11693

[11] King-Hele, D. G., Walker, D. M. C., "Evaluation of 15th- and 30th-Order Geopotential Harmonic Coefficients from 26 Resonant Satellite Orbits," *Planetary and Space Science*, Vol. 37, No. 7, July 1989, pp. 805–823.
doi:10.1016/0032-0633(89)90132-3

[12] Klokočník, J., Kostelecký, J., and Karasová, D., "*Satellite Altimetry and Its Use in Geoscience*," Vol. 40, Research Inst. of Geodesy, Topography And Cartography (VUGTK), Prague-Zdiby, Czech Republic, 1994, p. 157.

[13] Weigelt, M., Sideris, M. G., and Sneeuw, N., "On the Influence of the Ground Tracks on the Gravity Field Recovery from High-Low Satellite-to-Satellite Tracking Missions: CHAMP Monthly Gravity Field Recovery Using the Energy Balance Approach Revisited," *Journal of Geodesy*, Vol. 83, No. 12, 2009, pp. 1131–1143.
doi:10.1007/s00190-009-0330-5

[14] Klokočník, J., Kostelecký, J., and Gooding, R. H., "On Fine Orbit Selection for Particular Geodetic and Oceanographic Missions Involving Passage Through Resonances," *Journal of Geodesy*, Vol. 77, No. 1, 2003, pp. 30–40.
doi:10.1007/s00190-002-0276-3

[15] Reigber, C., Klokočník, J., Li, H., and Flechtner, F., "Contribution to ERS-1, Orbit Dossier, German PAF for ERS-1," Deutsches Geodätisches Forschungsinstitut, Munich, 1988.

[16] Lefebvre, M., and Vincent, R., "An Orbit Scenario Fitting Most of Constraints of Altimeter, SAR, and Scaterometer Missions, ERS 1 Sampling Capabilities," Centre National dEtudes Spatiales, Toulouse, France, 1988.

[17] Capderou, M., *Satellite Orbits and Missions*, Springer–Verlag, Paris, 2005, p. 364.

[18] Seidelmann, P. K., Archinal, B. A., A'hearn, M. F., Conrad, A., Consolmagno, G. J., Hestroffer, D., Hilton, J. L., Krasinsky, G. A., Neumann, G., Oberst, J., Stooke, P., Tedesco, E. F., Tholen, D. J., Thomas, P. C., and Williams, I. P., "Report of the IAU/IAG Working Group on Cartographic Coordinates and Rotational Elements 2006," *Celestial Mechanics and Dynamical Astronomy*, Vol. 98, No. 3, 2007, pp. 155–180.
doi:10.1007/s10569-007-9072-y

[19] Lemoine, F. G., Smith, D. E., Rowlands, D. D., Zuber, M. T., Neumann, G. A., and Chinn, D. S., "An Improved Solution of the Gravity Field of Mars (GMM-2B) from Mars Global Surveyor," *Journal of Geophysical Research*, Vol. 106, No. E10, 2001, pp. 23359–23376.
doi:10.1029/2000JE001426

[20] Marty, J. C., Balmino, G., Duron, J., Rosenblatt, P., Le Maistre, S., Rivoldini, A., Dehant, V., and Van Hoolst, T., "Martian Gravity Field Model and its Time Variations from MGS and Odyssey Data," *Planetary and Space Science*, Vol. 57, No. 3, 2009, pp. 350–363.
doi:10.1016/j.pss.2009.01.004

[21] Petrovskaya, M. S., and Vershkov, A. N., "Non-Singular Expressions for the Gravity Gradients in the Local North-Oriented and Orbital Reference Frames," *Journal of Geodesy*, Vol. 80, No. 3, 2006, pp. 117–127.
doi:10.1007/s00190-006-0031-2

[22] Konopliv, A. S., Banerdt, W. B., and Sjogren, W. L., "Venus Gravity: 180 Degree and Order Model," *Icarus*, Vol. 139, No. 1, 1999, pp. 3–18.
doi:10.1006/icar.1999.6086

[23] Lemoine, F. G., Smith, D. E., Zuber, M. T., Neumann, G. A., and Rowlands, D. D., "A 70th Degree Lunar Gravity Model (GLGM-2) from Clementine and Other Tracking Data," *Journal of Geophysical Research*, Vol. 102, No. E7, 1997, pp. 16339–16359.
doi:10.1029/97JE01418